Journal of Materials Chemistry B

Accepted Manuscript

ROYAL SOCIETY OF CHEMISTRY

www.rsc.org/materialsB

Journal Name

ARTICLE

BSA-coated magnetic nanoparticles for improved therapeutic properties

Received 00th January 20xx,
Accepted 00th January 20xx

DOI: 10.1039/x0xx00000x

www.rsc.org/

Antonio Aires,[a,b] Sandra M. Ocampo,[a] David Cabrera,[a] Leonor de la Cueva,[a] Gorka Salas,[a,b] Francisco J. Teran,[a,b,#] and Aitziber L. Cortajarena[a,b,#]

In recent years, magnetic nanoparticles have been widely investigated for their potential in biomedical applications. For successful *in vivo* application, magnetic nanoparticles must satisfy several requirements such as biocompatibility, invisibility to the immune system, high colloidal stability in biological fluids, and long blood circulation times. In this study, we have developed a formulation in which the magnetic nanoparticles are coated with bovine serum albumin to provide enhanced colloidal stability in biological fluids preserving their magnetic properties. In addition, the nanoparticles carry a chemotherapeutic drug, showing its potential as drug delivery system. Our results reveal the influence of protein adsorption on the colloidal stability and the dynamical magnetic response of functionalized magnetic nanoparticles. Moreover, cellular internalization and *in vitro* cytotoxic activity in Panc-1 pancreatic cancer cells provide evidences of improved cellular internalization, successful intracellular drug delivery, and efficient anticancer activity.

Introduction

Over the past 50 years, magnetic nanoparticles (MNP) have been widely investigated for their potential in biomedical applications. MNP may act as contrast agents or magnetic particle imaging tracers for imaging techniques,[1,2] nanocarriers for drug/gene-delivery,[3,4] and magnetic heating mediators for hyperthermia-based therapies.[5] MNP may simultaneously combine diagnostic and therapeutic properties. Among MNP, iron oxide nanoparticles (IONP) are the most employed nanocrystals due to their negligible toxicity and well-controlled synthetic routes. Thus, IONP engineering allows size-driven colloidal and magnetic properties.[6-8] The precise control of IONP size and coating engineering[8] favors their internalization into cells without cytotoxicity drawbacks.[9,10] An equally important aspect in the IONP design is to control their interaction with serum biomolecules leading to the formation of a protein corona when nanoparticles are suspended in biological fluids.[11-13] Serum protein adsorption phenomena have been studied under different perspectives, with many investigations focusing on the effect on cellular internalization and cytotoxicity of the nanostructures.[14,15] Many authors have shown that serum protein adsorption strongly changes the properties of the nanoparticles when dispersed in biological media.[16] The protein corona formation depends on the features of the nanoparticles such as morphology, porosity, crystallinity, roughness, or surface coating.[16-21] Physical properties of MNP are significantly altered after the formation of protein corona[17,22-24] resulting in changes in their colloidal stability that favour particle agglomeration.[25]

Another critical aspect related to MNP design for successful *in vivo* application is their invisibility to the immune system to avoid fast clearance by liver. The colloidal stability needs to be preserved and the blood circulation time of nanoformulations requires to be long enough to reach the target tissue in amounts suitable for therapeutic and/or detection purposes.[26,27] Different polymers coatings have been employed in recent years for improving these properties including poly(ethylene glycol) (PEG),[28,29] dextran,[30] chitosan,[31] poly(ethylenimine) (PEI),[32] and dimercaptosuccinic acid (DMSA).[33] Among the commonly-used polymeric materials, proteins or polypeptides are considered the most promising molecules as MNP protective coating layer due to their superior biocompatibility and hydrophilicity.[34] MNP coated with proteins can be synthesized through many methods, including simple adsorption,[35] photonic immobilization,[36] free-radical crosslinking,[37] sonochemical method,[38] and covalent immobilization.[39] When using proteins as coating agents, the preservation of the protein structure and activity is of great importance. Furthermore, it is essential to characterize the physical, magnetic, and functional properties of functionalized MNP under physiological conditions since they can strongly change in the biological environments in which are designed to act.

[a] IMDEA Nanociencia, Campus Universitario de Cantoblanco, 28049 Madrid, Spain
Email: aitziber.lopezcortajarena@imdea.org, francisco.teran@imdea.org
[b] Unidad Asociada de Nanobiotecnología CNB-CSIC & IMDEA Nanociencia, Campus Universitario de Cantoblanco, 28049 Madrid, Spain.
Electronic Supplementary Information (ESI) available. See
DOI: 10.1039/x0xx00000x

In this study, we have developed a multifunctionalized MNP (MF-MNP) formulation coated with the Bovine Serum Albumin protein (BSA) to improve the colloidal stability and magnetic response in biological fluids. Serum albumins are the major plasma proteins and have many physiological functions. BSA has been one of the most extensively studied proteins because of its sequence and structural homology with human serum albumin,[40] and could be considered the most promising protein for biocompatible coating of MNP for biomedical applications.[41] The preservation of the native structure of albumin upon its immobilization on the surface of nanoparticles provides MNP with hemocompatibility, longer blood circulation times, and hinders undesired adsorption of other proteins.[42] In addition, our formulation based on MNP includes gemcitabine (GEM) attached on the BSA coating, showing its additional potential as drug delivery system targeting pancreatic cancer cells. The effect of the surface functionalization on the colloidal stability and magnetic properties in different media, cellular internalization, and *in vitro* drug delivery into pancreatic cancer cells were investigated to evaluate their potential for *in vivo* application in controlled drug release and/or magnetic hyperthermia.

Materials and methods

Materials

All reagents were purchased from Aldrich and used without further purification. Ultrapure reagent grade water (18.2 MΩ, Wasserlab) was used in all experiments. Gemcitabine derivative, GEM-S-S-Pyr[43] was prepared according to described procedures.

Synthesis of magnetic nanoparticles

Dimercaptosuccinic acid (DMSA) coated magnetite nanoparticles (D-MNP) were prepared as follows. In a round-bottomed flask [Fe(acac)$_3$] (5.3 g, 15 mmol), oleic acid (12.7 g, 45 mmol) and 1,2-dodecanediol (6.1 g, 30 mmol) were mixed in 1-octadecene (150 mL). The reaction mixture was mechanically stirred (100 rpm) and warmed up with a heating mantle and the following temperature profile: i) 1.5°C/min from 25°C to 50°C, keeping the reaction at this temperature for 1 hour to have a homogeneous mixture, ii) 10°C/min until 220°C, keeping the reaction at this temperature for 30 minutes, iii) 1°C/min until 280°C, keeping the reaction at this temperature for 2 hours. The resulting black mixture was allowed to cool down to room temperature and washed several times with ethanol (10 x 40 mL) by centrifugation (relative centrifuge force (RCF) = 9000), separating the particles from supernatant with the aid of a permanent magnet. The resulting black residue is composed of hydrophobic nanoparticles of magnetite with a mean core size of 21 nm (s.d. = 3 nm). It was redispersed in hexane for storage. The iron concentration of the dispersion was measured by inductively coupled plasma optical emission spectrometry.

The water dispersion of D-MNP was prepared from the hexane MNP stock dispersion through a ligand substitution process with process with meso-2,3-dimercaptosuccinic acid as previously described.[33] The final D-MNP presented a zeta potential (ζ) = -57 ± 2 mV and a hydrodynamic diameter (D_H) = 60± 1nm. Magnetic properties of powder and frozen samples of D-MNP dispersed in water have been studied by vibrating that they are superparamagnetic at room temperature. The saturation magnetization of the powder at 298 K is 75 emu/g and the values of the frozen samples are 82 emu/g and 60 emu/g at 5 K and 250 K, respectively. Blocking temperature obtained from Zero Field Cooling-Field Cooling (ZFC-FC) measurements is around 260 K.

Functionalization of MNPs

Gemcitabine derivative, GEM-S-S-Pyr and dimercaptosuccinic acid coated MNP (D-MNP) functionalized with Gemcitabine (D-MNP-GEM) were prepared according to described procedures (Fig.1).[43]

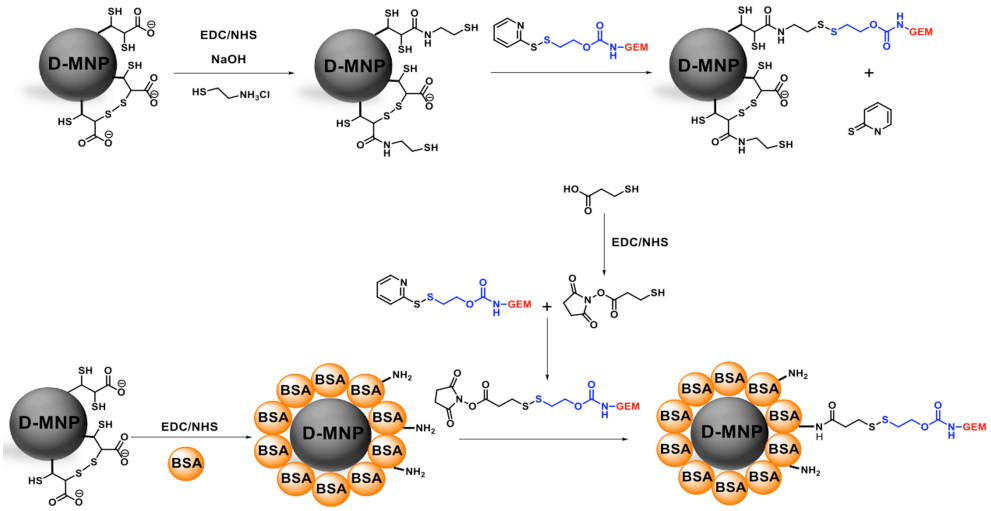

Fig. 1 General scheme of multifunctionalization of D-MNP.

For the functionalization of D-MNP with BSA and gemcitabine, we first start conjugating BSA protein. 5 mL of D-MNP at 2.4 mg Fe/mL were incubated 1 hour at room temperature with 150 µmol of EDC/g Fe and 75 µmol of NHS/g Fe. Then, the sample was washed by cycles of centrifugation and redispersion in milliQ 10 mM sodium phosphate buffer pH 7.4 (PB buffer) at least 3 times. These pre-activated D-MNP were incubated with different BSA solutions (83 µg BSA/mg Fe, 167 µg BSA/mg Fe and 250 µg BSA/mg Fe) in sodium phosphate buffer 10 mM (PB buffer), 4 h at room temperature and overnight at 4°C (Fig. 1). After that, the D-MNP coated with BSA (D-MNP-BSA) were purified by filtration thought a sepharose 6 CLB column using PB buffer. Samples of supernatants before and after the immobilization process were extracted and measured using Bradford assay.[44] The amount of bound BSA was determined as the difference between the remaining BSA concentration in the supernatant at ending of the immobilization process and the BSA concentration at the beginning of the immobilization process ($\mu g_{BSA}/mg_{Fe}$).

The D-MNP-BSA functionalization with Gemcitabine, prior required the pre-activation of the molecule. To a 800 µL of mercaptopropionic acid aqueous solution at 13.75 mM were added 100 µl of EDC at 0.21 M and 100 µL of NHS at 0.21 M. After addition, the reaction mixture was stirred for 2 hours at 40°C. Then, 1 mL of gemcitabine derivative solution at 10 mM in DMF was added and the resultant solution was stirred for 6 hour at 40°C (Fig. 1).

Finally, the D-MNP-BSA and the pre-activated gemcitabine react to obtain the final formulation. 5 mL of D-MNP-BSA at 2.4 mg Fe /mL suspension in PB buffer were mixed with 960 µL of 5 mM pre-activated gemcitabine derivative solution in DMF (0.48 µmol, 40 µmol/g Fe) during 16 h at 40°C (Fig. 1). After reaction, 200 µL of brine were added and the sample centrifuged 10 min at 10000xg. From the collected supernatants, the covalently immobilized GEM onto D-MNP-BSA was determined by quantification of the GEM by HPLC. Finally, the sample was re-dispersed in 5mL of PB buffer.

Colloidal characterization

Zeta potential and hydrodynamic size of the formulations were evaluated using a Zetasizer Nano-ZS instrument (Malvern Instruments). Hydrodynamic size value refers to the Z-average size and was measured by dynamic light scattering with a laser emitting red light at 633 nm as the energy source, and an angle of 173° between the sample and the detector. Zeta potential was measured at room temperature from dilute suspensions of the sample in water at 0.01 M of KNO_3 using a zeta potential cell. High-performance liquid chromatography (HPLC) was performed using a 1260 Infinity HPLC (Agilent Technologies) with a ZORBAX 300SB-C18 column 5 µm, 9.4 x 250mm. The colloidal stability of D-MNP-GEM and D-MNP-BSA-GEM formulation was evaluated in three different media: double distilled water (DDW), fetal bovine serum (FBS), and phosphate buffered saline (PBS). D_H of D-MNP-GEM and D-MNP-BSA-GEM were evaluated from dilute suspensions of the samples at 0.1 mg Fe/mL in DDW after incubating MF-MNP in different media at given iron content (1 mg_{Fe}/mL) for 5 min, 2, 4, 6, 8, and 24 h. MF-MNP were purified by filtration through a sepharose 6 CLB column.

Thermo Gravimetric Analysis

Thermo Gravimetric Analysis (TGA) of powdered samples was performed using an AQ-500 TA Instruments equipment. The analysis was designed at 100°C up to 1000°C fixing a heating rate of 10°C/min under a continuous flux of air (20 ml/min).

Magnetic characterization

The magnetic characterization of MNP (100 µL) under quasi-static conditions was carried out in a vibrating sample magnetometer (MLVSM9 MagLab 9 T, Oxford Instrument). Magnetization curves at 250 and 5 K were taken by saturating the sample in a field of 5 T. Saturation magnetization was evaluated by extrapolating to infinite field the experimental results obtained in the high field range where the magnetization linearly increases with 1/H. ZFC/FC data were obtained cooling the sample in a zero applied field (ZFC process) from room temperature to T = 5 K. Then, a field of H = 8 kA/m was applied and the magnetization of the sample was measured while increasing the temperature up to T = 260 K. After the last point was measured, the sample was cooled again to T = 5 K with the same applied field (FC process) and the magnetization increasing the temperature was measured. Coercitivity and remanent magnetization values are negligible at 250 K suggesting superparamagnetic–like behaviour at room temperatures. Under dynamical conditions (55 kHz and 32 kA/m), the magnetic characterization of MNP colloids were performed using a home-made inductive magnetometer set up similar to the one described by Mehdaoui, et al.[45] Alternating current (AC) magnetic field (H_{AC}) was generated by an air-cooled Litz wire coil. Inside this coil, two contrariwise-wounded compensated pick-up coils connected in series were set. Both pick-up coils have the same diameter and number of turns. The system quantifies the magnetic signal from MNP allowing to compare the magnetization cycles between MNP dispersed in different aqueous media under similar conditions (i.e. H_{AC} and iron content) to those employed for SAR measurements.

Calorimetric characterization

The specific absorption rate (*SAR*) values of MF-MNP were determined by non-adiabatic calorimetric measurements using reduced volumes of MNP dispersed in aqueous media.[46] Temperature changes after applying H_{AC} were monitored via a commercial optical fiber probe TS2/2 connected to a FOTEMP2-16 two-channel signal conditioner from Optocon AG with an experimental error of ±0.2°C. The experimental conditions employed to assess the heat dissipation power were similar for all different MNP dispersions: iron mass (36 μg_{Fe}), field conditions (185 kHz and 20 kA/m) and methodology (repeating three times the time variation temperature curves

of MNP dispersions after applying H_{AC} once thermal equilibrium is achieved). Thus, we extracted the values of the maximal slope at initial times after switching on H_{AC} (*i.e.* $dT/dt|_{max}$) for determining its average value and standard deviation. Afterwards, SAR values were determined by using the following expression:

(Equation 1) $$SAR = \frac{C_d m_d}{m_{Fe}} \frac{dT}{dt}\Big|_{\max}$$

where C_d is the volumetric specific heat of the dispersion media, m_d is the mass dispersion, m_{Fe} is the iron mass diluted in the dispersion, and $dT/dt\ |_{max}$ is the average value of the maximal slope at initial times after switching on H_{AC}. The volumetric specific heat constants of DDW, FBS, PBS were measured at the Servicio Interdepartamental de Investigación from Universidad Autónoma de Madrid obtaining the following values: C_{DDW}= 4.090 J/g°C, C_{FBS}= 3.984 J/g°C, C_{PBS}= 4.038 J/g°C.

Drug release from MNP

The release of GEM from the D-MNP-GEM and D-MNP-BSA-GEM was tested under physiological conditions (pH 7.4 and 37°C) using two different concentrations of reducing agent (1µM and 1mM of Dithiothreitol (DTT) to mimic the extracellular and intracellular conditions, respectively). For each experiment, 4.8 mg of D-MNP-GEM and D-MNP-BSA-GEM were dissolved in 1mL of PB buffer at pH 7.4 containing 1µM of DTT, or PB buffer containing 1mM DTT and incubated at 37°C. The amount of GEM released was analyzed at regular time intervals by HPLC using a C-18 column, mobile phase water/acetonitrile 80/20, at flow rate of 0.3 mL/min, measuring the absorbance at 270 nm. The percentage of GEM released was calculated from a standard calibration curve of free drug solution (Fig. S1 at ESI).

Cell culture and MNP incubation

Panc-1 cell line was purchased from American Type Culture Collections (Manassas, VA, USA). These cell lines were grown as monolayer in Dulbecco's Modified Eagle's Medium (DMEM) supplemented with FBS at a final concentration of 10%, 2mM L-glutamine, 0.25 µg/mL fungizone and 100 units of penicillin and 100µg/mL streptomycin. All the media, serum, L-glutamine, fungizone and antibiotics were purchased from GIBCO. Cell lines were maintained at 37°C in a humidified atmosphere consisting of 75% air and 5% CO_2 in an incubator. 500 µL of MNP dispersed in water was sonicated for redispersion purposes during 5 minutes. Then, MNP were diluted in medium containing 10% FBS at the desired concentration. The resulting sample was filtered through a 0.22 µm Millex-GP filter (Merck-Millipore Darmstadt, Germany) and sonicated again for 1 minute. Cells were incubated with MNP for 24h. Then, cell media with MNP dispersed was removed and cells were washed with phosphate buffered saline (PBS) for complete removal of MNP from cell medium. Then fresh cell media was added to continue further viability and internalization studies.

Internalization studies

In order to assess the internalization of D-MNP-GEM and D-MNP-BSA-GEM, Panc-1 cells were cultured on a 24-well plate at a density of $2.5x10^4$ cells per well in 500 µl of complete medium. After 24 h, the growth medium was removed and cells were then incubated 24 h at 37°C in the presence of D-MNP-GEM and D-MNP-BSA-GEM (50 µg Fe/mL). After incubation, cells were washed three times with PBS. Prussian blue staining of iron was performed to assess qualitatively the internalization of D-MNP-GEM and D-MNP-BSA-GEM into Panc-1 cells. For that purpose, cells were seeded on 12 mm square glass coverslips (Maienfeld GmbH & Co.KG, Germany) placed into the wells. Briefly, the cells were washed twice with PBS1x (AMRESCO, Ohio, USA) and fixed with 4 % paraformaldehyde solution for 30 min at room temperature. Again, cells were washed twice with PBS 1x, and were then incubated with a 1:1 mixture of 4% potassium ferrocyanide and 4% hydrochloric acid (Prussian blue staining solution) for 15 minutes at room temperature and washed with distilled water three times. The counterstaining was done for cytoplasm with neutral red 0.5% (Panreac Química S.L.U) for 2 minutes at room temperature and then washed with distilled water several times. After drying the cells, a cover slip was mounted by using DePeX (SERVA Electrophoresis GmbH) and finally, the cells were observed using light microscopy (Leica DMI-3000B, Leica Microsystems, Germany). All experiments were carried out in triplicate.

Inductively coupled plasma mass spectrometry (ICP-MS)

To determine the amount of MF-MNP internalized in Panc-1 cancer cell line, cells were seeded at 2.5×10^4 cells per well in 500 µl of DMEM containing 10% FBS. After 24 h, the growth medium was removed and cells were then incubated for 24 h at 37ºC in the presence of MF-MNP (0.2 mg Fe/mL). After incubation, cells were washed three times with phosphate-buffered saline (PBS), trypsinized with 200 µL of 0.25% w/v trypsin solution and were then incubated for 5 minutes at 37ºC. When a single cell suspension was obtained, 2 ml of complete media was added. The resultant solution was transferred to a sterile 15 mL conical centrifuge tube and spun down at 1200 rpm for 10 minutes. The supernatant was discarded carefully and cells were resuspended in 5 mL of fresh complete media and 100 µL was retained to count the cell number. The cell suspension was centrifuged again at 1200 rpm for 10 minutes and the supernatant was discarded carefully. 300 µL of 37% HCl was added to the cell pellet and the resultant suspension was sonicated for 30 minutes at 40ºC. Finally, 2700 µl of bi-distilled water was added. The iron concentration was determined by measuring the sample in ICP-MS NexION 300XX (Perkin Elmer) (n=2).

***In vitro* cytotoxicity assays**

Resazurin dye (Sigma-Aldrich) has been broadly used as a reliable indicator of cell viability in proliferation and cytotoxicity assays. To assess cell death, Panc-1 cells were cultured on a 24-well plate at a density of $2.5x10^4$ cells per well

in 500 µl of complete medium. After 24 h, the growth medium was removed and cells were then incubated 24 h at 37°C in the presence of different concentrations of free Gemcitabine (1, 0.20, 0.15 and 0.10 µM GEM), D-MNP and D-MNP-BSA (50, 9.2, 6.2 and 4.6 µg Fe/mL), D-MNP-GEM and D-MNP-BSA-GEM (50, 9.2, 6.2 and 4.6 µg Fe/mL corresponding to 1.0, 0.20, 0.15 and 0.10 µM GEM). After incubation, cells were washed three times with PBS, then DMEM supplemented with 10% FBS was added to cell culture, and maintained at 37°C and 5% CO_2 incubator. After 5 days, the medium was replaced with DMEM supplemented with 10% FBS, and 10% of Resazurin dye (1mg/ml PBS). Cells were maintained at 37°C and 5% CO_2 incubator for 3 hours and then, the amount of Resazurin reduced was determined by measuring the absorbance of the reaction mixture (λ_{exc}=570 nm, λ_{em}=600 nm) using a Synergy H4 microplate reader. 600 µl of 10% of resazurin dye was added to empty wells as a negative control. The viability of the cells was expressed as the percentage of absorption of treated cells in comparison with control cells (without nanoparticles). All experiments were carried out in triplicate. All the data obtained were plotted and statistically analyzed using the software package GraphPad Prism 5.0. All samples were compared using a one-way ANOVA and Bonferroni post-hoc test (*P < 0.05, **P < 0.01, and ***P < 0.001). Only significant differences among the samples are indicated in the charts.

Results and discussion

Multifunctionalization of MNP

The general strategy followed in order to prepare D-MNP-GEM and D-MNP-BSA-GEM is shown in Fig. 1. D-MNP-GEM were prepared according to described procedures.[43] The synthesis of D-MNP-GEM started by the reaction of cysteamine with the carboxylic groups of the DMSA coating in the presence of EDC and NHS. Then, a gemcitabine derivative was reacted with the activated D-MNP.[43] This conjugation was achieved employing 30 µmol of GEM derivative, leading to a formulation that contains 20 µmol GEM/g Fe (ζ= -46 ± 4 mV and a D_H = 61 ± 1 nm). The synthesis of D-MNP-BSA-GEM started by the covalent immobilization of the BSA onto the activated carboxylic groups of the DMSA coating with EDC and NHS. Then, D-MNP-BSA functionalization with gemcitabine was performed similarly to D-MNP-GEM. Different amounts of BSA were used with a fixed quantity of D-MNP. D-MNP-BSA-1, D-MNP-BSA-2, and D-MNP-BSA-3 formulations were prepared using 83 µg BSA/mg Fe, 167 µg BSA/mg Fe, and 250 µg BSA/mg. The results of the immobilization are summarized in Table S1. The number of BSA molecules/D-MNP was calculated considering the diameter of one D-MNP 22 nm, as measured by TEM (Fig. 2A). Using 83 µg BSA/mg Fe, a ratio of 7 BSA molecules/D-MNP was observed. Increasing the initial amount of protein to 167 µg BSA/mg Fe, derivative D-D-MNP-BSA-2 showed 13 BSA molecules/D-MNP. Finally, using 250 µg BSA/mg Fe (D-MNP-BSA-3), led to 14 BSA molecules/D-MNP indicating that the D-MNP at this stoichiometry is fully covered with BSA, as shown in TEM micrograph (Fig. 2). Fig. 2B shows a homogeneous layer of protein coating of about 4 nm surrounding the D-MNP core. This result is consistent with a uniform protein monolayer covering the D-MNP. Based upon results shown in Table S1, all the experiments were conducted with optimized D-MNP-BSA-3 (ζ= -42 ± 3 mV and D_H =68 ± 2 nm). The reaction of pre-activated Gemcitabine derivative with D-MNP-BSA led to a stable formulation. The immobilization yield of GEM was 50% with a load of 20 µmol GEM/g Fe (ζ = -40 ± 1 mV and D_H = 71 ± 1 nm). The colloidal stability, magnetic properties, stimuli-response behavior of D-MNP-GEM and D-MNP-BSA-GEM were investigated in order to assess the potential of the different MF-MNP formulations.

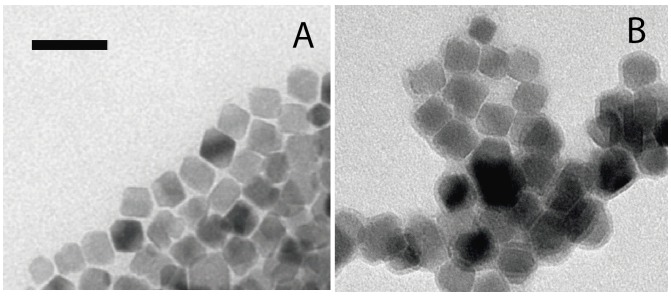

Fig. 2 TEM micrographs of D-MNP (A) and D-MNP-BSA (B). Scale bar corresponds to 50 nm.

Colloidal stability of MF-MNP

The colloidal stability was studied by dispersing MF-MNP in DDW, PBS, or FBS and monitoring D_H from MF-MNP. The changes of D_H from MF-MNP dispersed in different media are summarized in Fig. 3 and Tables 1, S2, S3 and S4.

These results indicated that in DDW dispersion, D-MNP-GEM and D-MNP-BSA-GEM had similar D_H and exhibited excellent stability with no significant aggregation. Contrary, D_H differently varied in PBS dispersion depending on the presence of BSA. D_H increased from 61±1 nm to 530±15 nm for D-MNP-GEM after 6 hours but did not significantly changed for D-MNP-BSA-GEM. The different aggregation state for both MF-MNP can be related to the electrostatic effect of the physiological salt concentration on the negative surface charge of the MF-MNP coating. D-MNP-GEM presents negative surface charge and DMSA coatinig molecules interact directly with the ions of PBS solution decreasing the repulsion forces between the D-MNP. This phenomenon leads to a major agglomeration process as observed in the value of D_H and its evolution with time (Fig. 3). For D-MNP-BSA-GEM, the presence of BSA screens the electrostatic interactions, and therefore no particle aggregation was observed. Finally, in FBS dispersion, D_H increased from 61±1 nm to 193±1 nm for D-MNP-GEM and from 71±1 nm to 169±2

Table 1. Hydrodynamic diameter of D-MNP-GEM and D-MNP-BSA-GEM in different media measured after 6 hours incubation time.

MF-MNP	DDW	PBS	FBS
D-MNP-GEM	61±1 nm	530±15 nm	193±1 nm
D-MNP-BSA-GEM	71±1 nm	75±2 nm	169±2 nm

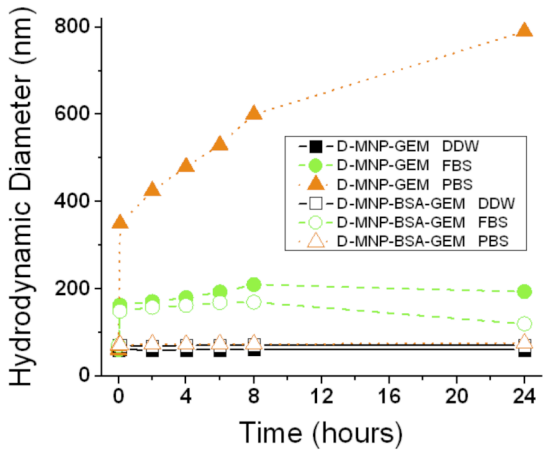

Fig. 3 Variation of hydrodynamic diameter of MF-MNP with time in different aqueous media. The hydrodynamic diameter of D-MNP-GEM (filled symbols) and D-MNP-BSA-GEM (empty symbols) was tested in DDW (black squares), FBS (green circles), and PBS (orange triangles) over 24 hours.

nm for D-MNP-BSA-GEM after 6 hours incubation. The increase in D_H can be related to protein adsorption and/or MNP aggregation. In order to determine which is the phenomenon behind the D_H increase in FBS, further TGA analysis was performed (Fig. S2 at ESI).

The presence of organic compounds on the surface of D-MNP can be quantified by TGA. In the case of D-MNP-GEM a weight loss of 5% was measured, which is related to the DMSA coating and the small fraction of GEM. However, when D-MNP-GEM was incubated in FBS for 6 hours, the weight loss increased to 67%. This increase is due to the protein adsorption (Table S3 and Fig. S2 at ESI). In the case of D-MNP-BSA-GEM, the weight loss curves showed 11% of organic content from the DMSA coating (5%) and the BSA covalently immobilized onto the surface of the D-MNP (6%). The weight loss was 70% after 6 hours of incubation in FBS leading to an increase of 59% of organic related to the protein adsorption phenomenon (Table 2 and Fig. S2 at ESI).

Table 2 shows that both formulations (D-MNP-GEM and D-MNP-BSA-GEM) increased similarly the percentage of organic after 6 hours of incubation in FBS (62% and 59%). However, significant differences between D_H and therefore the volumes of both formulations were measured after 6 hours of incubation in FBS ($3.8x10^6$ nm^3 and $2.5x10^6$ nm^3). If the increase in size were only due to protein adsorption, then a higher size would be expected for D-MNP-BSA-GEM than for D-MNP-GEM after incubation in FBS. As this is not the case a significant contribution to the size increase in D-MNP-GEM should be related to MNP aggregation. These results add evidence to support the enhanced colloidal stability of the BSA-coated MNP formulations and are in agreement with previous works that indicated the nanoparticle stabilizing effect of BSA.[35,47]

Table 2. Properties of D-MNP-GEM and D-MNP-BSA-GEM after 6 hours of incubation in DDW and FBS.

MF-MNP	Medium	D_H (nm)	Volume (nm^3)	% Organic
D-MNP-GEM	DDW	61	$1.1x10^5$	5
	FBS	193	$3.8x10^6$	67
D-MNP-BSA-GEM	DDW	71	$1.8x10^5$	11
	FBS	169	$2.5x10^6$	70

Magnetic properties of MF-MNP

We evaluated the influence of colloidal stability of the MF-MNP formulations on their dynamic magnetic response. We measured SAR values and AC hysteresis loops from MF-MNP at 1 mg_{Fe}/mL iron content and different H_{AC} conditions in order to determine changes in the AC magnetic responses (see Materials and methods). First, we determined the heating capacity of the MF-MNP dispersed in different aqueous media. Recent works have shown that the heating efficiency is a suitable physical parameter to test the colloidal stability of nanoparticle dispersions in terms of MNP aggregation.[22,48-50] In this work, we evaluated the effect on the SAR value when the hydrodynamic size increases due to aggregation or adsorption of molecules onto the MF-MNP surface. Fig. 4 shows the comparison of SAR values obtained under similar experimental conditions (H_{AC} and iron content) from the different MF-MNP formulations dispersed in different media. At a first glance, the heating efficiency showed significant differences depending on the presence of BSA coating and the dispersion media. Thus, D-MNP-BSA-GEM (red bars) showed comparable values in all aqueous dispersions, contrary to D-MNP-GEM (blue bars). Indeed, this latest formulation showed significantly different SAR values depending on the dispersion media. The relative comparison between D-MNP-BSA-GEM and D-MNP-GEM led to similar SAR values in DDW, 25% lower SAR values for D-MNP-GEM than for DMSA-BSA-GEM in FBS, and much lower SAR values for D-MNP-GEM in PBS where colloid precipitation is observed after few minutes, reflecting a big uncertainty on the measured SAR value.

The differences in the heat dissipation are in agreement with previous studies[22] and can be understood in terms of their colloidal stability of MF - MNP formulations in different

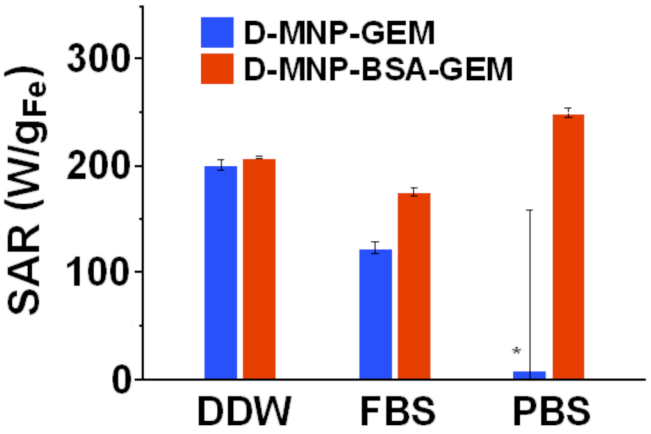

Fig. 4 SAR values of the different MF-MNP dispersed in distinct aqueous media, DDW, FBS, and PBS. SAR values were measured at similar iron content (1 mg_{Fe}/ml) and AC magnetic field conditions (185 kHz and 20 kA/m). *Value obtained under unstable colloidal conditions after 5 minutes of preparation. The error bars correspond to standard deviation.

aqueous media. In DDW, both MF-MNP formulations have similar colloidal stability (*i.e.* D_H) and therefore, their heating efficiency is similar. In PBS, the colloidal stability is highly related to the presence of BSA coating, as discussed above, thus the absence of BSA coating led to MNP precipitation due to large aggregation (Table 1). In FBS, an intermediate situation was observed with a decrease of the SAR values with respect to the values obtained in DDW, being more significant in absence of BSA coating due to the different colloidal stability in FBS media related to the presence of BSA coating (Table 1, Fig. 3). It is worth to note that such stability is probably associated with the generation of an organic protein corona around the MF-MNP, that is more significant in the absence of BSA coating.

The heat dissipation values obtained for the MF-MNP formulations dispersed in different media revealed the sensitivity of the dynamical magnetic response of MNP to the colloidal stability in agreement with DLS or TGA results. Another relevant information from the AC magnetic response of MNP is provided by the hysteresis loops. Since SAR values are related to the area of hysteresis loops (A) by the expression SAR=$A \cdot f$, we can study how the physical parameters associated to A (*i.e.* coercitive field, H_C and remanent magnetization, M_R) are influenced by colloidal stability in the different aqueous media. Fig. 5 shows the AC hysteresis loops from different MF-MNP formulations dispersed in different aqueous media.

In case of MF-MNP dispersed in PBS, BSA plays an important role defining the shape of hysteresis loops (i.e. values of H_C and M_R). Indeed, hysteresis loops seem to have a better developed A and larger H_C and MR values for D-MNP-BSA-GEM in all aqueous media. These results are in agreement with the larger SAR values obtained for D-MNP-BSA-GEM compared to MF-MNP without BSA coating. In addition, the presence of BSA coating led to hysteresis loops that only change in FBS media contrary to D-MNP-GEM for which hysteresis loops are different in FBS and PBS media with respect to DDW. These experimental evidences reflect the key role of BSA coating in supplying optimal colloidal stability in aqueous media with physiological salt and protein concentrations. TGA results indicate that for D-MNP-GEM, organic adsorption and/or MNP aggregation are behind the changes in SAR values and hysteretic shapes. Whereas in the case of D-MNP-BSA-GEM, the organic adsorption is responsible of the changes of SAR and hysteresis in FBS media. This is an interesting result that reflects the sensitivity of AC magnetic response to the adsorption of biomolecules onto MNP surface. Similar results related to the formation of protein corona have been observed in quasi-static magnetization measurements and longitudinal and transverse relaxivities of the superparamagnetic iron oxide MNP.[23,24]

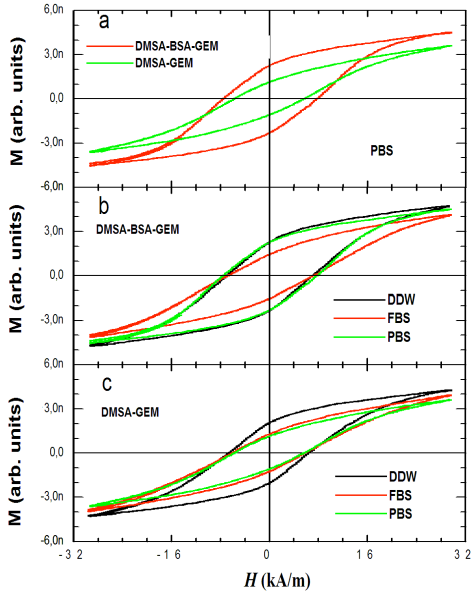

Fig. 5 AC hysteresis loops measured in a) MF-MNP formulations dispersed in PBS, b) D-MNP-BSA-GEM dispersed in different aqueous media, c) D-MNP-GEM dispersed in different aqueous media. All measurements were performed at 1 mg Fe/ml iron content and AC magnetic field conditions of 55 kHz and 32 kA/m.

Drugs release studies

First, we studied the release of gemcitabine from D-MNP-GEM and D-MNP-BSA-GEM in two different concentrations of reducing agent, 1 μM and 1 mM of DTT to mimic the extracellular and intracellular environments respectively (Fig. 6). Similar release pattern was observed for both formulations, with 94-96% release when treated with 1 mM DTT after 6-8 h while only 3-6% of the cargo was released with 1 μM DTT after 6-8 h (Fig. 6). These results show that the release rate of GEM from D-MNP-GEMand D-MNP-BSA-GEM strongly depends on the reducing environment so that it will take place mostly intracellularly, in the cytoplasm and lysosomal environments and that the release is not affected by the presence of the BSA coating.

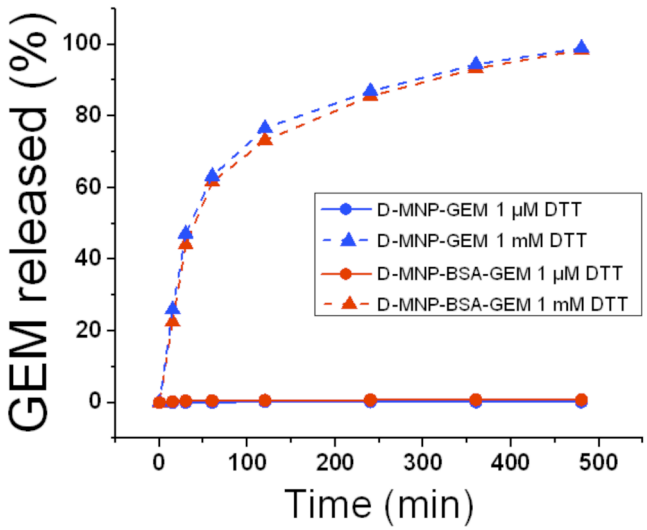

Fig. 6 Release kinetics of Gemcitabine from D-MNP-GEM (blue triangles and dashed line, 1mM DTT and, blue circles, and solid line, 1μM DTT) and D-MNP-BSA-GEM (red triangles and dashed line, 1mM DTT and, red circles ans solid line, 1μM DTT).

In vitro internalization and cytotoxicity studies

Gemcitabine is a chemotherapeutic drug currently used in clinic for the treatment of pancreatic cancer, therefore we used pancreatic cancer cells to test the drug delivery capabilities of the nanoformulations. The internalization of D-MNP-GEM and D-MNP-BSA-GEM into pancreatic cancer cells (Panc-1) was investigated by cell incubation for 24 h at 37°C, followed by several washes with PBS and Prussian blue staining to monitor the presence of iron from the MF-MNP. As shown in Fig. 7, in the case of D-MNP-BSA-GEM more MNP were detected by Prussian blue staining than in the case of D-MNP-GEM, under the same experimental conditions. The amount of MF-MNP internalized in Panc-1 cancer cell line was quantified by ICP-MS, showing 21 ± 2 pg of Fe/cell for D-MNP-BSA-GEM, and 5 ± 2 pg of Fe/cell cells in the case of D-MNP-GEM.

These results suggest that D-MNP-BSA-GEM are more stable in the culture media than D-MNP-GEM and therefore could be internalized in larger amounts. The cytotoxicity effect of the D-MNP-GEM and D-MNP-BSA-GEM compared to free GEM was evaluated on the pancreatic cell line (Panc-1) using Alamar Blue assay. The initial incubation was performed during 24 hours at 37°C. Then, cells were washed with PBS incubated for 5 days at 37°C.

In the cytotoxicity studies, we observed that the MNP without drug do not show any toxic effect (Fig. 8), which confirms the biocompatibility of both formulations and that the functionalization with BSA does not induce any toxicity. At the highest concentration of drug tested (1μM) similar antiproliferative activity was observed for the free GEM and both GEM-functionalized MNP formulations with and without BSA coating (Fig. 8). However at the lowest drug concentrations (0.20 μM, 0.15 μM and 0.10 μM) there were significant differences between free GEM, D-MNP-GEM and D-MNP-BSA-GEM. D-MNP-BSA-GEM showed similar antiproliferative activity than the free drug, whereas D-MNP-GEM showed significantly less activity. These results confirm that the higher internalization rate of D-MNP-BSA-GEM led to an increase in the drug delivery and therefore in its cytotoxic efficacy. *In vitro* cytotoxicity studies on pancreatic cancer cells line (Panc-1) indicate that D-MNP-BSA-GEM is an efficient formulation for cancer therapy with satisfied biocompatibility.

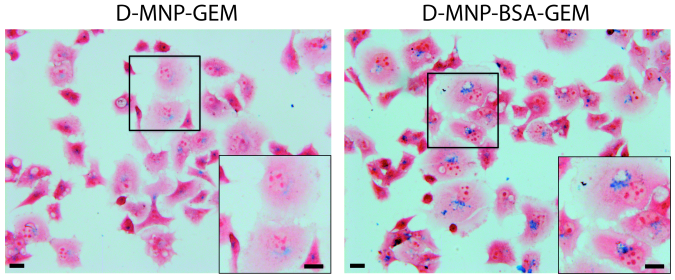

Fig. 7 Prussian blue staining of Panc-1 cells incubated with D-MNP-GEM and D-MNP-BSA-GEM (scale bar = 20 μm).

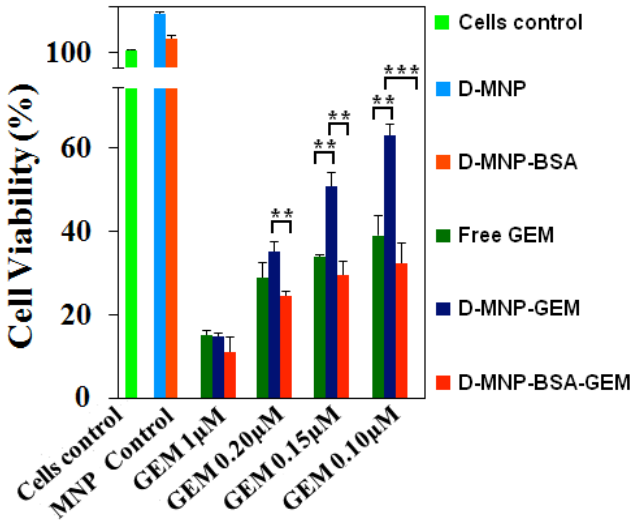

Fig. 8 Viability of Panc-1 cells control and treated with free Gemcitabine (1.00, 0.20, 0.15 and 0.10 μM) and D-MNP, D-MNP-BSA (50μg_{Fe}/mL), D-MNP-GEM (1.00, 0.20, 0.15 and 0.10 μM), D-MNP-BSA-GEM (1.00, 0.20, 0.15 and 0.10 μM). (*P < 0.05, **P < 0.01, and ***P < 0.001).

Conclusions

In this work, we have used a biocompatible protein coating in order to improve the physical, magnetic, and functional properties of a therapeutic formulation based on magnetic iron oxide nanoparticles under physiological conditions. On one hand, we have characterized in detail the colloidal and magnetic properties of the MNP formulation functionalized with gemcitabine under physiological conditions. Our results show that the protein coating improves the colloidal properties under physiological conditions, significantly reducing MNP aggregation and consequently, increasing their stability over time. The increased colloidal stability favors the preservation of the magnetic response in physiological media such as FBS and PBS. On the other hand, the biocompatibility of MF-MNP was assessed in PANC-1 cancer cell line revealing that BSA protein coating improves their cellular uptake and therefore increases the chemotherapeutic effect of gemcitabine. We have shown that BSA-coating improves *in vitro* therapeutic outcome of MF-MNP for efficient cancer treatment. These *in vitro* results highlight the potential of BSA coating MF-MNP for successful *in vivo* studies.

Acknowledgements

This work has been partially supported by European Commission (MULTIFUN, nº 262943), Comunidad de Madrid NANOFRONTMAG-CM project (S2013/MIT-2850), and Spanish Ministry of Economy and Competitiveness (MAT2013-47395-C4-3-R). F.J.T. acknowledges the European COST Action TD1402 (RADIOMAG) and the financial support from Ramon y Cajal subprogram (RYC-2011-09617).

References

1 P. Hahn, D. Stark, J. Lewis, S. Saini, G. Elizondo, R. Weissleder, C. Fretz and J. Ferrucci, *Radiology*, 1990, **175**, 6.
2 H. Arami, R. M. Ferguson, A. P. Khandhar and K. M. Krishnan, *Medical Physics*, 2013, **40**, 071904.
3 J. Dobson, *Gene Therapy*, 2006, **13**, 283-287.
4 R. Mejías, S. Pérez-Yagüe, L. Gutiérrez, L. I. Cabrera, R. Spada, P. Acedo, C. J. Serna, F. J. Lázaro, Á. Villanueva, M. d. P. Morales and D. F. Barber, *Biomaterials*, 2011, **32**, 2938-2952.
5 K. Maier-Hauff, F. Ulrich, D. Nestler, H. Niehoff, P. Wust, B. Thiesen, H. Orawa, V. Budach and A. Jordan, *Journal of neuro-oncology*, 2011, **103**, 317-324.
6 R. Costo, V. Bello, C. Robic, M. Port, J. F. Marco, M. Puerto Morales and S. Veintemillas-Verdaguer, *Langmuir*, 2012, **28**, 178-185.
7 G. Salas, S. Veintemillas-Verdaguer and M. d. P. Morales, *International Journal of Hyperthermia*, 2013, **29**, 768-776.
8 Y. Luengo, S. Nardecchia, M. P. Morales and M. C. Serrano, *Nanoscale*, 2013, **5**, 11428-11437.
9 M. Calero, L. Gutiérrrez, G. Salas, Y. Luengo, A. Lázaro, P. Acedo, M. P. Morales, R. Miranda and A. Villanueva, *Nanomedicine : nanotechnology, biology, and medicine*, 2013.
10 A. Prina-Mello, K. Crosbie-Staunton, G. Salas, M. del Puerto Morales and Y. Volkov, *Magnetics, IEEE Transactions on*, 2013, **49**, 377-382.
11 U. Sakulkhu, L. Maurizi, M. Mahmoudi, M. Motazacker, M. Vries, A. Gramoun, M.-G. Ollivier Beuzelin, J.-P. Vallee, F. Rezaee and H. Hofmann, *Nanoscale*, 2014, **6**, 11439-11450.
12 C. Gunawan, M. Lim, C. P. Marquis and R. Amal, *Journal of Materials Chemistry B*, 2014, **2**, 2060-2083.
13 E. Casals, T. Pfaller, A. Duschl, G. J. Oostingh and V. Puntes, *ACS Nano*, 2010, **4**, 3623-3632.
14 L. Treuel, S. Brandholt, P. Maffre, S. Wiegele, L. Shang and G. U. Nienhaus, *ACS Nano*, 2014, **8**, 503-513.
15 W. Hu, C. Peng, M. Lv, X. Li, Y. Zhang, N. Chen, C. Fan and Q. Huang, *ACS Nano*, 2011, **5**, 3693-3700.
16 A. Salvati, A. S. Pitek, M. P. Monopoli, K. Prapainop, F. B. Bombelli, D. R. Hristov, P. M. Kelly, C. Aberg, E. Mahon and K. A. Dawson, *Nat Nano*, 2013, **8**, 137-143.
17 D. Eberbeck, M. Kettering, C. Bergemann, P. Zirpel, I. Hilger and L. Trahms, *Journal of Physics D: Applied Physics*, 2010, **43**, 405002.
18 M. Lundqvist, I. Sethson and B.-H. Jonsson, *Langmuir*, 2004, **20**, 10639-10647.
19 Q. Mu, Z. Li, X. Li, S. R. Mishra, B. Zhang, Z. Si, L. Yang, W. Jiang and B. Yan, *The Journal of Physical Chemistry C*, 2009, **113**, 5390-5395.
20 A. Nel, T. Xia, L. Mädler and N. Li, *Science*, 2006, **311**, 622-627.
21 A. A. Vertegel, R. W. Siegel and J. S. Dordick, *Langmuir*, 2004, **20**, 6800-6807.
22 A. P. Khandhar, R. M. Ferguson and K. M. Krishnan, *Journal of applied physics*, 2011, **109**, 07B310.
23 H. Amiri, L. Bordonali, A. Lascialfari, S. Wan, M. P. Monopoli, I. Lynch, S. Laurent and M. Mahmoudi, *Nanoscale*, 2013, **5**, 8656-8665.
24 H. T. R. Wiogo, M. Lim, V. Bulmus, L. Gutiérrez, R. C. Woodward and R. Amal, *Langmuir*, 2012, **28**, 4346-4356.
25 A. Petri-Fink, B. Steitz, A. Finka, J. Salaklang and H. Hofmann, *European Journal of Pharmaceutics and Biopharmaceutics*, 2008, **68**, 129-137.
26 E. Valero, S. Fiorini, S. Tambalo, H. Busquier, J. Callejas-Fernández, P. Marzola, N. Gálvez and J. M. Domínguez-Vera, *Journal of Medicinal Chemistry*, 2014, **57**, 5686-5692.
27 R. Venerando, G. Miotto, M. Magro, M. Dallan, D. Baratella, E. Bonaiuto, R. Zboril and F. Vianello, *The Journal of Physical Chemistry C*, 2013, **117**, 20320-20331.
28 K. Hervé, L. Douziech-Eyrolles, E. Munnier, S. Cohen-Jonathan, M. Soucé, H. Marchais, P. Limelette, F. Warmont, M. L. Saboungi, P. Dubois and I. Chourpa, *Nanotechnology*, 2008, **19**, 465608.
29 J. Y. Park, P. Daksha, G. H. Lee, S. Woo and Y. Chang, *Nanotechnology*, 2008, **19**, 365603.
30 S. Mornet, J. Portier and E. Duguet, *Journal of Magnetism and Magnetic Materials*, 2005, **293**, 127-134.
31 K. Donadel, M. D. V. Felisberto, V. T. Fávere, M. Rigoni, N. J. Batistela and M. C. M. Laranjeira, *Materials Science and Engineering: C*, 2008, **28**, 509-514.
32 I.-K. Park, C.-P. Ng, J. Wang, B. Chu, C. Yuan, S. Zhang and S. H. Pun, *Biomaterials*, 2008, **29**, 724-732.
33 G. Salas, C. Casado, F. J. Teran, R. Miranda, C. J. Serna and M. P. Morales, *Journal of Materials Chemistry*, 2012, **22**, 21065-21075.
34 Z. Li, L. Qiang, S. Zhong, H. Wang and X. Cui, *Colloids and Surfaces A: Physicochemical and Engineering Aspects*, 2013, **436**, 1145-1151.
35 S.-M. Yu, A. Laromaine and A. Roig, *Journal of Nanoparticle Research*, 2014, **16**, 1-15.
36 A. Parracino, G. P. Gajula, A. K. di Gennaro, M. Correia, M. T. Neves-Petersen, J. Rafaelsen and S. B. Petersen, *Biotechnology and Bioengineering*, 2011, **108**, 999-1010.
37 A. V. Bychkova, M. A. Rosenfeld, V. B. Leonova, O. N. Sorokina, S. M. Lomakin and A. L. Kovarski, *Colloid Journal*, 2013, **75**, 7-13.
38 C. E. Bunker, K. C. Novak, E. A. Guliants, B. A. Harruff, M. J. Meziani, Y. Lin and Y.-P. Sun, *Langmuir*, 2007, **23**, 10342-10347.
39 R. V. Mehta, R. V. Upadhyay, S. W. Charles and C. N. Ramchand, *Biotechnology Techniques*, 1997, **11**, 493-496.
40 T. Peters Jr, in *Advances in Protein Chemistry*, eds. J. T. E. C.B. Anfinsen and M. R. Frederic, Academic Press1985, vol. Volume 37, pp. 161-245.
41 A. O. Elzoghby, W. M. Samy and N. A. Elgindy, *Journal of controlled release,* 2012, **157**, 168-182.
42 I. Lynch, A. Salvati and K. A. Dawson, *Nat Nanotechnol*, 2009, **4**, 546-547.
43 A. Latorre, P. Couleaud, A. Aires, A. L. Cortajarena and Á. Somoza, *European Journal of Medicinal Chemistry*, 2014, **82**, 355-362.
44 M. M. Bradford, *Analytical Biochemistry*, 1976, **72**, 248-254.
45 B. Mehdaoui, J. Carrey, M. Stadler, A. Cornejo, C. Nayral, F. Delpech, B. Chaudret and M. Respaud, *Applied Physics Letters*, 2012, **100**, 052403.
46 F. J. Teran, C. Casado, N. Mikuszeit, G. Salas, A. Bollero, M. P. Morales, J. Camarero and R. Miranda, *Applied Physics Letters*, 2012, **101**, 062413.
47 A. Bajaj, B. Samanta, H. Yan, D. J. Jerry and V. M. Rotello, *J. Mater. Chem*, 2009, **19**, 6328-6331.
48 M. E. de Sousa, M. B. Fernández van Raap, P. C. Rivas, P. Mendoza Zélis, P. Girardin, G. A. Pasquevich, J. L. Alessandrini, D. Muraca and F. H. Sánchez, *The Journal of Physical Chemistry C*, 2013, **117**, 5436-5445.
49 G. Salas, J. Camarero, D. Cabrera, H. Takacs, M. Varela, R. Ludwig, H. Dähring, I. Hilger, R. Miranda, M. d. P. Morales and F. J. Teran, *The Journal of Physical Chemistry C*, 2014, **118**, 19985-19994.
50 M. L. Etheridge, K. R. Hurley, J. Zhang, S. Jeon, H. L. Ring, C. Hogan, C. L. Haynes, M. Garwood and J. C. Bischof, *TECHNOLOGY*, 2014, **02**, 214-228.

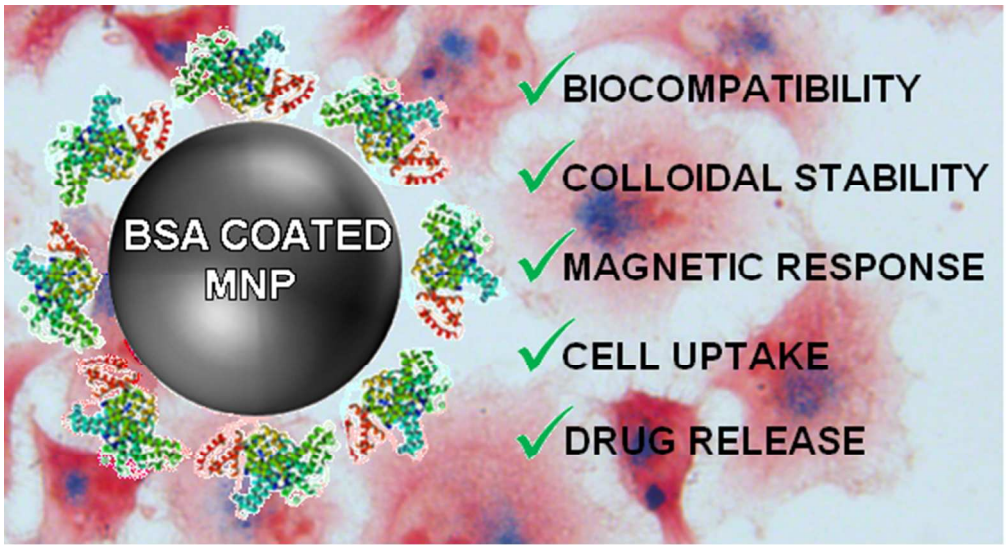

Albumin coating improves stabillity of magnetic nanoparticles under physiological conditions, favoring their magnetic properties, cellular uptake, and chemotherapeutic effect.
160x86mm (96 x 96 DPI)